

Interference pattern in the collision of structures in the BEC dark matter model: comparison with fluids

J. A. González¹ and F. S. Guzmán¹

¹*Instituto de Física y Matemáticas, Universidad Michoacana de San Nicolás de Hidalgo. Edificio C-3, Cd. Universitaria, C. P. 58040 Morelia, Michoacán, México.*

(Dated: January 20, 2013)

In order to explore nonlinear effects on the distribution of matter during collisions within the Bose-Einstein condensate (BEC) dark matter model driven by the Schrödinger-Poisson system of equations, we study the head-on collision of structures and focus on the interference pattern formation in the density of matter during the collision process. We explore the possibility that the collision of two structures of fluid matter modeled with an ideal gas equation of state also forms interference patterns and found a negative result. Given that a fluid is the most common flavor of dark matter models, we conclude that one fingerprint of the BEC dark matter model is the pattern formation in the density during a collision of structures.

PACS numbers: 95.35.+d, 05.30.Jp, 03.75.Lm, 05.45.Yv

I. INTRODUCTION

The discovery of the nature of dark matter is one of the most important problems nowadays, and a considerable amount of theoretical models have been proposed. One of the candidates that has received certain attention is a scalar field dark matter ultralight particle that is consistent with cosmological observations [1, 2]. At cosmological scales, this and other related models have been widely studied, and one of the important issues to be understood about this candidate is its behavior at local scales related to nonlinear processes of collapse, structure formation and collision of structures. Some theoretical studies have pushed forward this model at local scales, especially those related to galactic rotation curves under various conditions [3–5]. In the case of ultralight scalar fields, it has been shown that the density profiles of scalar field structures is not cuspy as opposed to Navarro Frenk White density profiles [6], and also predicts an adequate cutoff in the mass power spectrum of structures consistent with the abundance of small structures [2]. Finally, more recently the evolution of cosmological perturbations in Bose-Einstein condensate dark matter is already under study [7].

In the nonlinear regime, some advances have been made related to the evolution of gravitating scalar field structures, both relativistic under general relativistic conditions [8] and Newtonian in the low energy and weak gravitational field regime [9–12].

The Newtonian case has been found to be more appropriate to study the nonlinear collapse and interaction between structures, and is driven by the time-dependent Schrödinger-Poisson (SP) system of equations. The interpretation of this system of equations is that Schrödinger equation represents a Bose-Einstein condensate (BEC) of the scalar field particles at zero temperature in the mean field approximation, through the Gross-Pitaevskii equation [13]. This is the reason why in the low energy and weak gravitational field limits, the scalar field dark

matter model is called BEC dark matter.

The solution of the time-dependent SP system requires the application of numerical methods to visualize the evolution of BEC structures and estimate any potential observable implication. A helpful feature of the SP system is that it has equilibrium configurations, that is, there are spherically symmetric stationary solutions based on the assumption that the wave function depends harmonically in time, which in turn implies that both the gravitational potential and the energy density are time-independent [9, 10]. Such equilibrium configurations have been studied dynamically and found to be stable under spherical perturbations and are also attractor solutions in time for initial perturbations with arbitrary profile [10]; they are also stable against nonspherical perturbations [11], and they serve as stable structures to study how BEC dark matter structures behave in nonlinear situations.

In this paper, we explore the BEC dark matter model during the head-on collision of structures as depicted first in [12], where it was found that when the binary system is initially bounded, the resulting system is a single object, whereas for unbounded systems a sort of solitonic behavior was shown to happen. In both cases, it was found that an interference pattern was formed during the collision which potentially would provide predictions on the behavior of baryonic matter whose stream would be driven in part by the dark matter gravitational potential during the collision of two structures.

On the other hand, the most studied models of dark matter assume it can be a dust fluid, which is an approximate model of dark matter candidates like WIMPs. Thus, in this work we present a comparison of the head-on collision of two structures assuming on the one hand that the structures correspond to two equilibrium configurations of the Schrödinger-Poisson system and on the other hand the structures correspond to two relaxed balls of ideal gas.

The goal is to determine whether or not the collision of two balls of gas representing two structures of WIMPs can also present an interference pattern during the head-

on collision, and thus conclude that the BEC dark matter has peculiar fingerprint interference patterns during the collision of structures that should predict observations that determine its viability, or determine the BEC dark matter should be ruled out.

This paper is organized as follows: In Sec. II we introduce the systems of equations we solve, and the numerical methods we use in order to carry out the head-on collision of two structures, both of BEC dark matter and of an ideal gas; in Sec. III we present the results of our simulations and compare the behavior in the two cases; and finally in Sec. IV we draw some conclusions.

II. SYSTEMS OF EQUATIONS AND NUMERICAL METHODS

A. The Schrödinger-Poisson system

The system of equations. The SP system of equations consists of the Schrödinger equation for a wave function ψ , with a potential that is solution of Poisson equation sourced by the density of probability $|\psi|^2$. Since we deal with a head-on collision, we write down the SP system in cylindrical coordinates as follows:

$$\begin{aligned} i\frac{\partial\psi}{\partial t} &= -\frac{1}{2}\left(\frac{\partial^2\psi}{\partial x^2} + \frac{1}{x}\frac{\partial\psi}{\partial x} + \frac{\partial^2\psi}{\partial z^2}\right) + U\psi + \Lambda|\psi|^2\psi \\ \frac{\partial^2 U}{\partial x^2} + \frac{1}{x}\frac{\partial U}{\partial x} + \frac{\partial^2 U}{\partial z^2} &= \psi^*\psi, \end{aligned} \quad (2)$$

where $\psi = \psi(x, z, t)$ and $U = U(x, z, t)$ are the wave function and the gravitational potential respectively; x, z are the radial and axial cylindrical coordinates respectively. The third order term in Eq. (1) is related to a self-interacting term, in which Λ corresponds to the s-wave scattering length in the Gross-Pitaevskii approximation for Bose condensates [13], which we set to zero in this work, because it is irrelevant in the interference pattern formation studied here. This term instead was shown to play the role of determining the compactness of an equilibrium configuration [10]. Eqs. (1-2) use the units and scaling $\hbar = c = 1$ with $x \rightarrow mx$, $z \rightarrow mz$, $t \rightarrow mt$ and the wave function $\psi \rightarrow \sqrt{4\pi G}\psi$, where m is the mass of the ultralight boson. A consequence of this change of units is that the mass of a system will be in units of $[M] = M_{pl}^2/m$, and thus m determines the scale of the configurations we start with. In fact these units define the Kaup mass, which in the relativistic counterpart of the Schrödinger-Poisson system (the boson star case ruled by the Einstein-Klein-Gordon system of equations) indicates the threshold between stable and unstable bounded configurations [14]. It is worth mentioning that in the case of the Schrödinger-Poisson system, that is, the low energy and weak field limits of boson stars, the equilibrium configurations are all stable, unless a negative self-interaction factor Λ is introduced [10].

The evolution of the system. We consider the system (1-2) to be a constrained evolution system, that is the Schrödinger equation is an evolution equation that satisfies the Poisson equation which is a constraint. Explicitly, we integrate the Schrödinger equation using a finite differences approximation along the spatial directions and a method of lines for the integration in time that uses a third order Runge-Kutta algorithm. We solve the constraint (Poisson equation) at the intermediate steps of the time integrator, which provides a full coupling of the evolution constrained system, as shown in our convergence tests. The flow of the solution is as follows: at every intermediate iteration of the Runge-Kutta integrator: i) evolve the system using the Schrödinger equation to evolve ψ , ii) use such updated value of the wave function to source and solve the Poisson equation, iii) then obtain a new potential U and repeat. Usually the Schrödinger equation is integrated in time using unitary operators [15], which is related to fully implicit methods, however, even though we use explicit methods we verified the evolution is unitary as shown in [10–12]. In order to avoid the singularity at $x = 0$ in Eqs. (1-2) with our finite differences approximation, we stagger the axis such that we avoid the origin, and in order to achieve the second order convergence at the axis we use the identity $\frac{1}{x}\frac{\partial f}{\partial x} = 2\frac{df}{dx^2}$, and code the later expression, which is a derivative with respect to x^2 .

Poisson equation. Eq. (2) is an elliptic equation for U which we solve using the 2D five-point stencil for the derivatives and a successive over-relaxation iterative algorithm with optimal acceleration parameter [16]. In order to impose boundary conditions we made sure the boundaries are far enough for the number of particles represented by the integral of the density of probability $N = \int |\psi|^2 d^3x$ to be the same along the boundary of the domain and used a monopolar term of the gravitational field; that is, we used the value $U = -N/r$ along the boundaries with $r = \sqrt{x^2 + z^2}$. At the axis we demand the gravitational potential to be symmetric with respect to the axis.

Boundary conditions during the evolution. We use a sponge in the outermost region of the domain. The sponge is a concept used with success in the past when dealing with the Schrödinger equation [17, 18]. This technique consists in adding up to the potential in the Schrödinger equation an imaginary part. The result is that in the region where this is applied there is a sink of particles, and therefore the density of probability in this region will be damped out, with which we get the effects of an outgoing flux boundary condition [18]. The expression we use for the sponge profile is

$$V = -\frac{i}{2}V_0 \{2 + \tanh[(r_{jk} - r_c)/\delta] - \tanh(r_c/\delta)\}, \quad (3)$$

which is a smooth version of a step function with amplitude V_0 , centered at r_c and width δ ; $r_{jk} = \sqrt{x_{jk}^2 + z_{jk}^2}$ is the radius of a given point of the discretized domain; the

minus sign guarantees the decay of the number of particles at the outer parts of our integration domain, that is, the imaginary potential behaves as a sink of particles.

Initial data. In order to reduce our parameter space to specific but illustrative cases, we only consider the equal mass head-on collision case. Thus we construct the solution of a spherically symmetric equilibrium ground state configuration in spherical coordinates as done in [9, 10, 18]. In the units used the mass of each configuration is $N = 2.06$ with a radius containing the 95% of the total mass is $x_{95} = 3.93$ [18]. We obtain a wave function ψ_{sph} and gravitational potential U_{sph} . We then interpolate such wave function at two different places of the two-dimensional grid $(0, \pm z_0)$ centered along the z -axis and define a global wave function $\psi = \psi_1 + \psi_2$, where ψ_1 and ψ_2 are the wave functions obtained from the spherical solution located at two different places of the 2D grid. We choose z_0 such that the two configurations are far enough one from the other so that the interference term $\langle \psi_1, \psi_2 \rangle$ lies near to round off error values, in order to consider the two blobs have the adequate phase; the magnitude of this term decreases exponentially with the initial separation of the blobs. In this way, we solve the Poisson equation sourced by the energy density $\rho = |\psi|^2$. Then we have initial data for two superposed ground state equilibrium configurations in our axially symmetric domain.

Analysis. In order to analyze the kinetic development of the collision it is important to track global quantities during the evolution, such as kinetic, gravitational and total energy. We do this by calculating the expectation values

$$K = -\frac{1}{2} \int \psi^* \nabla^2 \psi d^3x, \quad (4)$$

$$W = \frac{1}{2} \int \psi^* U \psi d^3x, \quad (5)$$

which are respectively the expectation values of the kinetic and gravitational energies. These quantities are important at determining the state of the system at any time during the evolution of the system. For instance, the value of the total energy $E = K + W$ indicates whether we account with a bounded system or not, and the very important virial theorem relation $2K + W = 0$, which is nearly satisfied when the system gets virialized and relaxed through whatever channels available, for instance, the emission of scalar field bursts, the so-called gravitational cooling process [19].

B. The SPH algorithm for the fluid

We want to study the head-on collision of two structures of ideal gas. In order to do that, we need to solve Euler's equations coupled to Newtonian gravity. With this in mind, we implemented a smoothed particle hydrodynamic (SPH) code based on the formulation described

in [20]. This scheme allows us to evolve the position, velocity, density, pressure and internal energy of the fluid elements. We explore two different scenarios of ideal. In the first one we set the internal energy and pressure equal to zero, and in the second one we use the more general ideal gas equation of state $p = (\Gamma - 1)\rho u$, where p is the pressure of the gas, ρ is its density, Γ is a constant and u is the internal energy of the gas.

Initial data. The initial values required for our simulations are the positions, velocities, density, pressure and internal energy of the particles in the fluid.

We start choosing the density profile given by the Plummer model:

$$\rho(r) = \frac{3M}{4\pi R^3} \left(1 + \frac{r^2}{R^2}\right)^{-5/2}, \quad (6)$$

for the fluid without pressure and the density profile:

$$\rho(r) = \frac{M}{2\pi R^2} \frac{1}{r}, \quad (7)$$

for the fluid with pressure.

We construct one of the structures using an acceptance-rejection method to generate the position of the particles in such a way that they satisfy the corresponding density profile. We set the initial velocities of the particles equal to zero and set the parameters $M = 2.0622$ and $R = 3.93$. Finally, we set the value of the internal energy equal to a constant ($u = 0$ for the pressureless fluid and $u = 0.05M/R$ in the other case) and recover the pressure from the equation of state. Such configurations are not in equilibrium, therefore we evolve them numerically and let them settle down into an equilibrium state.

In order to generate the initial data corresponding to the head-on collision of two bumps of fluid, we take the resulting equilibrium configuration described in the previous paragraph, make two copies of it and place them at a given separation along the z -axis. Then a boost on each of the configurations is applied along the head-on axis. The initial positions are $z = \pm 10.0$ and the initial velocity is $v_z^0 = \pm 2.6875/2.0622$. This value was chosen such that the total energy of the system is equal to zero, although other values of the boost were explored and the results are qualitatively the same.

III. RESULTS

We perform a series of head-on collisions of two initial balls in both cases, the one driven by the SP system of equations and the fluid driven by hydrodynamics. We set up configuration for the SP system and for the fluid that are dynamically comparable in time, size and separation. The reason is that there is no way to identify exactly an initial configuration corresponding to the quantum

mechanical system driven by the Schrödinger equation (which is dispersive) with the configurations constructed for an ideal gas.

We define the total energy of the system as $E = K + W$, where K and W are the expectation values of the kinetic gravitational energies defined in (4-5), calculated with the time-dependent wave function that is being calculated on the fly of the Schrödinger-Poisson system, and $E = K + U + W$ is the total energy, that is the sum of the kinetic, internal and gravitational energies in the case of the fluid. The total energy depends strongly on the value of the initial head-on momentum the initial balls have, so that we choose this parameter to be the one we tune in order to obtain our initial binary configurations.

The parameter space we explore corresponds to initial configurations with different values of the total energy E , which allows to explore situations in which the system is both bounded ($E < 0$) and unbounded ($E > 0$).

We consider there is a pattern formation if there is a sequence of strips of the density of matter of the size of the order of the initial radii of the initial configurations as shown to happen during the collision of two blobs of BEC [12].

A. Bose condensate initial configurations

We choose two ground state spherically symmetric equilibrium configurations that are originally virialized, that is, they satisfy separately the condition $2K + W = 0$ and superpose them into the 2d grid (for details in the construction of equilibrium configurations see [18]). We apply momentum along the head-on direction in the following way: assume $\psi = \psi_1 + \psi_2$ is the wave function resulting from the superposition of the two equilibrium configurations, where ψ_1 and ψ_2 represent the wave function of each of the two equilibrium configurations centered along the head-on axis z at $\pm z_0$, being ψ_1 and ψ_2 centered at $-z_0$ and z_0 respectively. Thus we add up momentum to each of the configurations defining a new wave function $\psi = e^{ip_z} \psi_1 + e^{-ip_z} \psi_2$. After this process we solve Poisson equation and start the evolution.

According to the Gross-Pitaevskii theory, BECs behave like classical waves, and as such interference phenomena are expected. Experiments showing interference patterns are well known [21]. In these experiments two separate Bose condensate configurations are released from their respective traps and allow them to evolve freely; eventually the two densities of probability interfere and produce a total density of the form

$$|\psi_1 + \psi_2|^2 = |\psi_1|^2 + |\psi_2|^2 + 2 \langle \psi_1, \psi_2 \rangle \cos \left(\frac{md}{\hbar t} + \Phi \right), \quad (8)$$

where m is the mass parameter in Schrödinger's equation, and d is the initial distance between the two condensates, and Φ is the initial phase difference between the two condensates given by $\psi = \psi_1 + e^{i\Phi} \psi_2$, which is nonzero when

there is a nonzero head-on initial momentum. The density of probability (8) predicts a spacing between two consecutive fringes of constructive interference given by

$$\lambda = \frac{\hbar t}{md}, \quad (9)$$

which in our units corresponds to $\lambda = 2\pi t/d = 2\pi t/(2z_0)$. This type of pattern formation has also been verified with simulations of laboratory systems (see e.g. [22]). We have to remind the reader that an important difference between the conditions in these experiments and our system is that we actually never release the condensates from their respective traps which are the gravitational potentials the density of probability generates, instead, we allow the traps to interact with each other. Nevertheless we use the formula to measure the distance between fringes and find that for big values of the initial head-on momentum p_z , that is, a big value of Φ in the experiments, the law is nearly valid, whereas for small phases it does not hold. We interpret this result as a consequence of the fact that for the cases where the head-on momentum is small, a merger is actually expected to occur and the interaction between the traps becomes important, whereas in the high momentum a nearly solitonic trespassing effect happens.

The parameter space we consider is shown in Table I and snapshots of pattern formation are shown in Fig. 1. Notice that the width of the energy density in the patterns is even thicker than the initial size of the equilibrium configurations at initial time.

p_z	sgn(E)	time for collision	λ given by (9)	λ (measured)
0.0	-	~ 43	13.5	2.9
0.3	-	~ 21	6.59	2.8
0.5	-	~ 16	5.03	2.7
0.7	0	~ 13	3.99	2.3
1.5	+	~ 6.5	2.01	1.8
2.5	+	~ 4.3	1.27	1.2

TABLE I: Parameters of the initial configurations for the BEC case. We also show the value of the distance between fringes of interference both, as predicted by formula (9) for laboratory experiments and the one we measure.

We perform our calculations using the domain $x \in [0, 20]$, $z \in [-20, 20]$ and a uniformly discretized grid, with constant time resolution Δt and the same resolution along both spatial directions $\Delta x = \Delta z = \Delta xz$ and a sponge radius with $r_c = 17$ and $\delta = 1$. In order to validate our numerical results we show in Fig. 2 a criterion that shows our results converge. As mentioned above, we use a method of lines with second order stencils along the spatial directions and a third order accurate integrator in time, so that we expect the code to converge to second order at least. Since we have no exact solution to our problem to compare with, or a constraint of the PDE system of equations

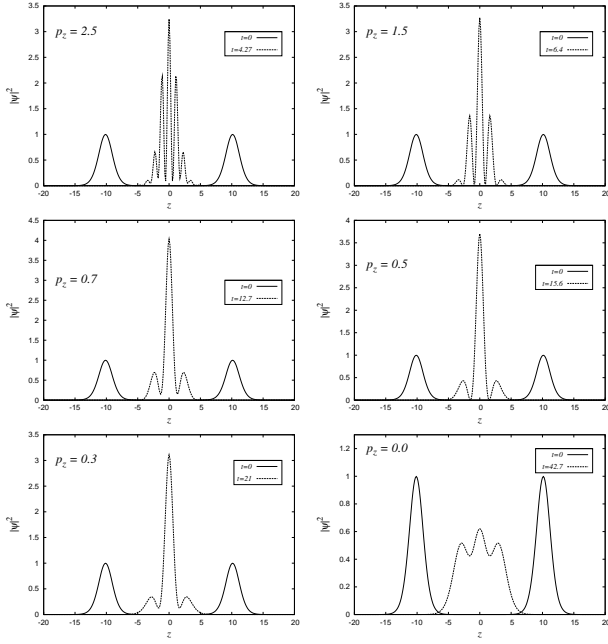


FIG. 1: We show the best snapshot of the density $|\psi|^2$ along the z axis showing the interference pattern. We also show the initial value of the density, in order to compare the size of the interference pattern.

we should expect to be satisfied, we can only practice a self-convergence test, that is, we use three different resolutions $\Delta x z_1 = 0.2$, $\Delta x z_2 = 0.13333 = \Delta x z_1/1.5$ and $\Delta x z_3 = 0.08888 = \Delta x z_2/1.5$ and track the maximum of the energy density $\rho_{bec} = |\psi|^2$, which corresponds to the infinity norm of ρ_{bec} because it is always non-negative. Given the ratio between our resolutions is 1.5, we expect the maximum of the density to satisfy

$$\frac{\max(\rho_{bec}[\text{using } \Delta x_1]) - \max(\rho_{bec}[\text{using } \Delta x_2])}{\max(\rho_{bec}[\text{using } \Delta x_2]) - \max(\rho_{bec}[\text{using } \Delta x_3])} = 1.5^Q, \quad (10)$$

where Q is the order of convergence expected to hold, which is at least two in our case because such is the order of accuracy of our stencils along the spatial directions and at most three, which is the accuracy of our time integrator. In Fig. 2 we also show the value of Q . In all our calculations we kept the factor $\Delta t/\Delta x z^2 = 0.1$ constant for all the resolutions, which maintains the evolution stable, accurate and convergent.

B. Fluid configurations

We evolve the initial configurations of fluid integrating Euler's equations using a predictor-corrector scheme. We compute the total, kinetic, potential and internal energy of the system in order to monitor the behavior of our numerical evolution.

The first case we analyzed is the pressureless fluid. In

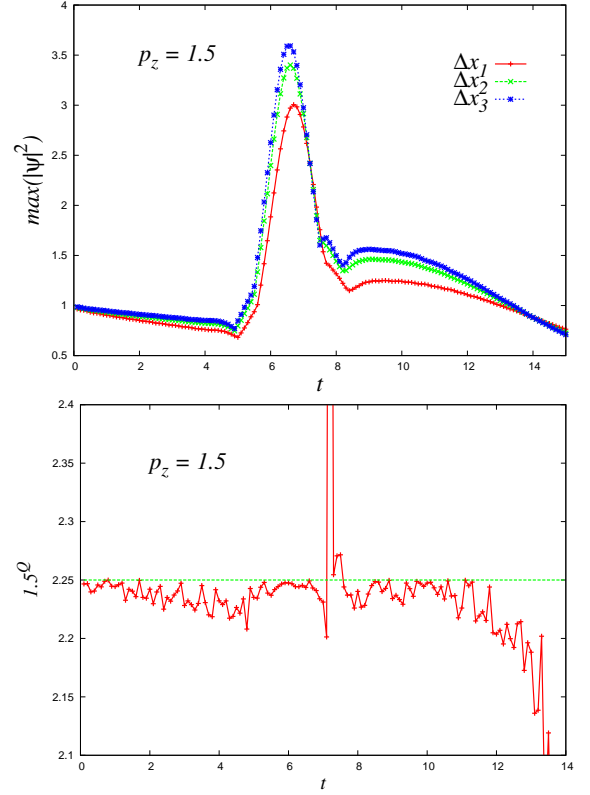


FIG. 2: (Top) In order to show the convergence of our algorithms we track the maximum of the energy density during the evolution for the particular case $p_z = 1.5$, which would be equivalent to estimate the infinity norm of the energy density. In our calculations we used three different resolutions $\Delta x_1 = 0.2$, $\Delta x_2 = \Delta x_1/1.5$ and $\Delta x_3 = \Delta x_2/1.5$. (Bottom) We show the convergence factor, that is 1.5^Q , which in theory should be $1.5^2 = 2.25$ for a second order convergent implementation. We show how much our calculations approach second order convergence; the convergence factor oscillates usually near or around the theoretical value due to phases in the scalar (the maximum of the density in our case) for the various resolutions. A big peak also appears approximately by the time the density approaches its maximum, and we see how convergence is lost after around $t \sim 11$ and decreases clearly afterwards by the time the blobs reach the sponge region, where the calculations are not expected to converge since there Schrödinger's equation has been modified with an artificial sink of particles, and also the unitarity of the evolution in the numerical domain is lost.

Fig. 3 we show snapshots at different times of the density as function of the z -position of the particles. The time of collision is around $t \sim 7.2$ and it is clear that no interference pattern is generated during such a collision. In Fig. 4 we show the kinetic, potential, internal and total energy of the system, in which it can be noticed that no internal energy is being involved in the model.

The second case is the ideal gas case with pressure. As before, in Fig. 5 we present the density as function of the position for different times and in Fig. 6 the energies of the system. In this scenario, again, we were unable to

track any interference patterns. These figures illustrate the role played by the pressure, which produces the density profiles to be less steep compared to the pressureless case.

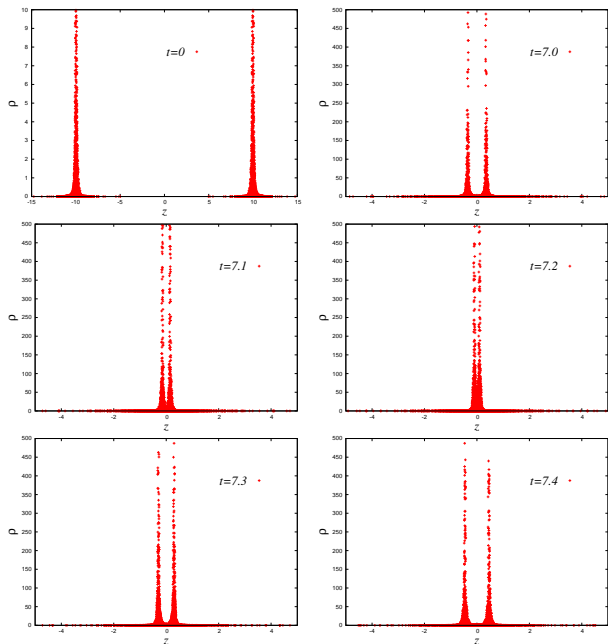


FIG. 3: In this plot we show snapshots at different times of the density as function of the z coordinate of the structures of an ideal gas with zero pressure. The collision takes place after $t \sim 7.2$. The evolution shows that the fluids cross each other without showing any pattern of interference

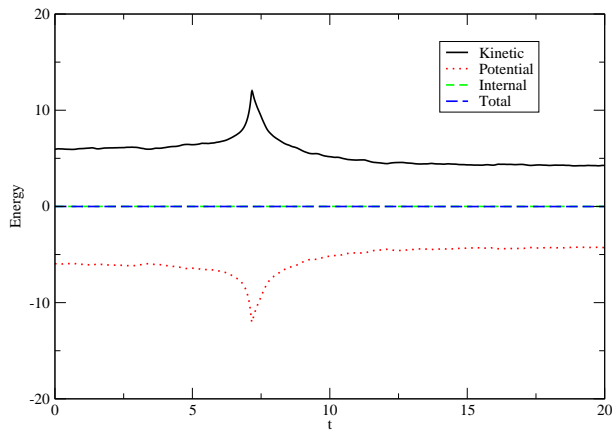


FIG. 4: In this plot we show the total, kinetic, potential and thermal energy for the head-on collision of the pressureless fluid configurations. The peak appears approximately by the time the density of the fluid reaches its maximum.

We have also performed simulations with various values of the initial linear momentum in the head-on direction and thus various values of the total energy of the system. We have also carried out our simulations with various numbers of particles and in all the cases the re-

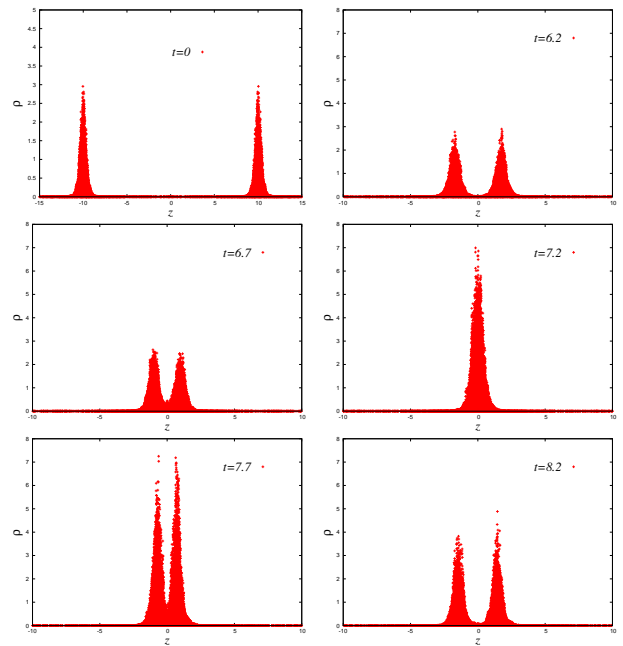


FIG. 5: In this plot we show snapshots at different times of the density as function of the z coordinate of the structures of fluid. As in the pressureless case, the evolution shows the

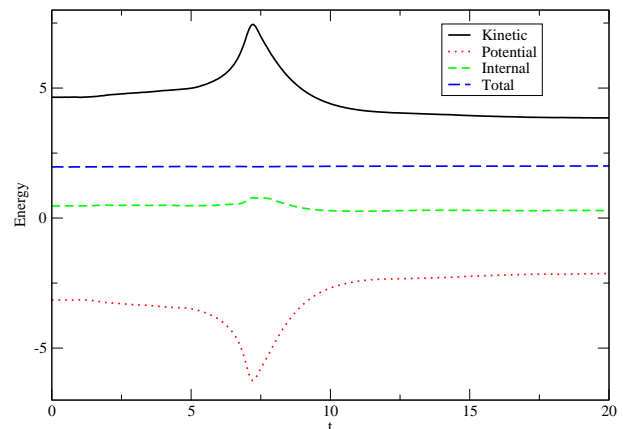


FIG. 6: In this plot we show the total, kinetic, potential and thermal energy for the head-on collision of fluid with pressure.

sults are qualitatively the same.

IV. CONCLUSIONS

We have solved the SP system as the equations describing the evolution of gravitating Bose condensates, which represents the BEC dark matter model and its properties at local scales. We have focused on the head-on collision of two equilibrium ground state configurations, and studied the interference pattern formation of the density of the configuration during the collision.

In order to investigate whether or not other type of fluids may show a similar interference pattern, we also studied the collision of two spherical configurations made of an ideal gas fluid, both with and without pressure using SPH techniques for different values of the total energy.

We found that the pattern formation during the collision of structures does not happen for the fluid. This leads to the conclusion that a fingerprint of the BEC dark matter model is the presence of interference patterns during the collision of structures. That is, if evidence of such interference patterns is not found, the BEC dark matter

model should be ruled out.

Acknowledgments

This work is supported by Grant Nos. CIC-UMSNH-4.9 and 4.23, PROMEP UMICH-CA-22, UMICH-PTC-210, CONACyT 79601 and 106466. Our simulations were carried out in the IFM Cluster.

-
- [1] V. Sahni, L. Wang, Phys. Rev. D **62**, 103517 (2000).
 - [2] T. Matos, L. A. Urena-Lopez, Phys. Rev. **D 63**, 063506 (2001).
 - [3] Jae-weon Lee, In-guy Koh, Phys.Rev. D53 (1996) 2236-2239.
 - [4] F. Siddhartha Guzman, Tonatiuh Matos, Class.Quant.Grav.17:L9-L16,2000. T. Matos, F. S. Guzman, D. Nunez, Phys.Rev.D62:061301,2000. K. K. Nandi, I. Valitov, N. G. Migranov, Phys.Rev.D80:047301,2009.
 - [5] A. Arbey, J. Lesgourgues and P. Salati, Phys. Rev. D **64**, 123528 (2001). A. Arbey, J. Lesgourgues and P. Salati, Phys. Rev. D **65**, 083514 (2002).
 - [6] A. Bernal, T. Matos, D. Nunez, Rev. Mex. A&A **44**, 149 (2008).
 - [7] T. Harko, arXiv:1101.3655v2 [gr-qc].
 - [8] M. Alcubierre, F. S. Guzman, T. Matos, D. Nunez, L. A. Urena-Lopez and P. Wiederhold, Class. Quantum Grav. **19**, 5017 (2002).
 - [9] F. S. Guzman, L. A. Urena-Lopez, Phys. Rev. D **68**, 024023 (2003).
 - [10] F. S. Guzman, L. A. Urena-Lopez, ApJ. **645**, 814 (2006).
 - [11] A. Bernal, F. S. Guzman, Phys. Rev. **D 74**, 063504 (2006).
 - [12] A. Bernal, F. S. Guzman, Phys. Rev. **D 74**, 103002 (2006). Jae-Weon Lee, Sooil Lim, Dale Choi, arXiv:0805.3827v1 [hep-ph].
 - [13] L. P. Pitaevskii, Zh. Eksp. Teor. Fiz. **40**, 646 (1961) [Sov. Phys. JETP **13**, 451 (1961)]. E. P. Gross, J. Math. Phys. **4**, 195 (1963).
 - [14] D. J. Kaup, Phys. Rev. **172**, 1331 (1968)
 - [15] D. I. Choi, 1998, Ph D Thesis, The University of Texas at Austin. D. I. Choi, Phys. Rev **A 66**, 063609 (2002).
 - [16] Smith G. D., 1965. Numerical Solution of Partial Differential Equations, Oxford University Press.
 - [17] M. Israeli and S. A. Orszag, J. Comp. Phys. **41**, 115 (1981).
 - [18] F. S. Guzman, L. A. Urena-Lopez, Phys. Rev. D **69**, 124033 (2004).
 - [19] Edward Seidel, Wai-Mo Suen, Phys.Rev.Lett.72:2516-2519,1994.
 - [20] Stephan Rosswog New Astronomy Reviews:**53**, 78 (2009)
 - [21] M. R. Andrews, C. G. Towsend et al., Science **275** (1997) 637.
 - [22] A. Röhrli, M. Narashevski, A. Schenzle and H. Wallis, Phys. Rev. Lett. **78** (1997) 4143.